

Axion Haloscope Array With \mathcal{PT} Symmetry

Yifan Chen^a, Minyuan Jiang^{b,a}, Yiqiu Ma^c, Jing Shu^{a,d,e,f,g,h}, and Yuting Yang^{a,d}

^aCAS Key Laboratory of Theoretical Physics, Institute of Theoretical Physics,
Chinese Academy of Sciences, Beijing 100190, P.R.China

^bWeizmann Institute of Science, Rehovot 76100, Israel

^cCenter for Gravitational Experiment, School of Physics,
Huazhong University of Science and Technology, Wuhan, 430074, China

^dSchool of Physical Sciences, University of Chinese Academy of Sciences, Beijing 100049, China

^eCAS Center for Excellence in Particle Physics, Beijing 100049, China

^fSchool of Fundamental Physics and Mathematical Sciences, Hangzhou Institute for Advanced Study,
University of Chinese Academy of Sciences, Hangzhou 310024, China

^gCenter for High Energy Physics, Peking University, Beijing 100871, China

^hInternational Center for Theoretical Physics Asia-Pacific, Beijing/Hangzhou, China

(Dated: May 25, 2022)

We generalize the recently proposed \mathcal{PT} -symmetric axion haloscope to a larger array with more \mathcal{PT} -symmetric structures. The optimized signal-to-noise ratio (SNR) has a greater enhancement, as well as the signal power. Furthermore, we show that the robustness of the detector towards the variations of the array coupling is the strongest when a binary tree structure is introduced which contains a largely enhanced \mathcal{PT} symmetry. The multiple allowed probing sensors can further increase the SNR by a factor of sensors' number due to the correlation of the signals. This type of array can strongly boost the search for axion compared to single mode resonant detection. The enhancement to the SNR becomes the most manifest when applied to the newly proposed detection using superconducting radiofrequency cavity with AC magnetic field where most of the parameter space of the QCD axion above kHz can be probed.

Introduction— Axion, with initial motivation to solve the strong CP problem in QCD [1], is a strongly motivated hypothetical particle beyond the standard model. Besides the QCD-axion, axion-like particles (ALPs) also appear generically in theories with extra dimensions [2]. These particles can be ideal candidates of cold dark matter [3–5], behaving like a coherent wave within the correlation time and distance. There are many strategies to search for axion dark matter, for example, using resonant microwave cavity or superconducting circuit as haloscope [6–8], axion-induced birefringence effect for light propagation [9–11] and axion-induced nuclear magnetic precession [12–14]. The main experimental platforms include ADMX [15], SN1987A [16] and CAST [17], which set the current limits to the axion parameters.

The strategy using resonant microwave system is based on the axion-photon interaction (so-called inverse Primakoff process) in a strong background magnetic fields, which was first discussed by Sikivie [6, 7]. The original haloscope includes a microwave cavity embedded in a DC magnetic field, including ADMX [15], ORGAN [18], HAYSTACK [19] and CAPP [20]. Generalizations targeted at different axion mass include superconducting-LC circuits [8] like DM radio [21] and ABRACADABRA [22] as well as superconducting radiofrequency (SRF) cavity embedded in the AC magnetic field [23].

Since the microwave field generated by axion conversion is extremely weak, a microwave resonator with high quality factor (Q -factor) is essential for the experiment, which at the same time narrows the bandwidth of the detector. Therefore, to search for the axion dark matter

in a broad mass spectrum, we need to switch the detector among different central frequencies in the practical running of the detector. The figure of merit for the Sikivie-type axion haloscope with tunable center frequency is the scan-rate R_a , defined as [24]:

$$R_a = \int_0^\infty d\Omega \frac{1}{|S_\alpha(\Omega)|^2}, \quad (1)$$

where $S_\alpha(\Omega)$ is the sensitivity (noise normalized by the signal amplitude) of the Haloscope. Here we assume the axion coherence time is short compared to the observation time.

To improve the scan-rate, one can either reduce the system noise-level, or broadening the detection bandwidth (at the same time does not sacrifice the sensitivity). Several works targeted at reducing the system noise-level [23–29] has been carried, for example, microwave squeezing technology is useful in improving the scan-rate. Recently, a new design [30] which has the feature of \mathcal{PT} symmetry is proposed to substantially broaden the detector bandwidth and thereby significantly reduces the switching time costs. The basic structure of this new proposal is the Sikivie type axion detector assisted with auxiliary non-degenerate parametric amplification, which was inspired by the white light cavity concept used in Laser Interferometer Gravitational Wave Detectors [31].

Haloscope with \mathcal{PT} symmetry— The detector design with \mathcal{PT} -symmetric feature in [30], shown in Fig. (1), can be described by the following interaction

Hamiltonian:

$$\hat{H}_{\text{int}}/\hbar = g(\hat{a}\hat{b}^\dagger + \hat{a}^\dagger\hat{b}) + G(\hat{b}\hat{c} + \hat{b}^\dagger\hat{c}^\dagger) + \alpha(\hat{a} + \hat{a}^\dagger)\Phi, \quad (2)$$

where $\hat{a}, \hat{b}, \hat{c}$ are three cavity modes. The mode \hat{a} is used to probe the axion signal Φ with coupling constant α , while the mode \hat{b} is connected to the readout port where we extract the detection result. There are two different kinds of interaction in this Hamiltonian, (1) the beam-splitter type interaction with strength g between modes \hat{a} and \hat{b} ; (2) non-degenerate parametric interaction [32, 33] with strength G between modes \hat{b} and \hat{c} . These modes couple with external continuous fields via :

$$\hat{H}_{\text{ext}}/\hbar = i\sqrt{2\gamma_a}(\hat{a}\hat{u}_a^\dagger - \hat{a}^\dagger\hat{u}_a), \quad (3)$$

and it takes the same form for \hat{b}, \hat{c} modes.

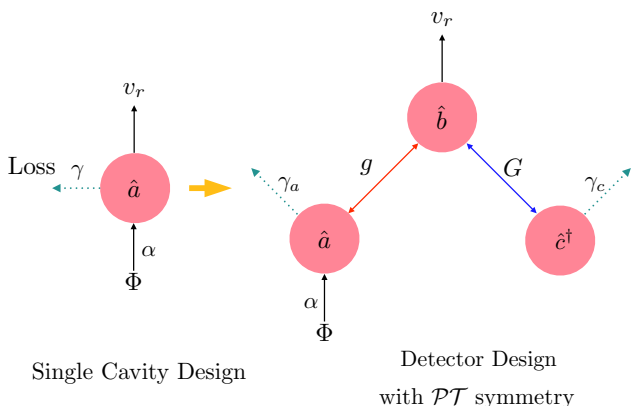


FIG. 1: Design concept of the detector with \mathcal{PT} symmetry (when $g = G$), where two auxiliary degrees of freedom were introduced with beam splitter and parametric types of interaction in red and blue, respectively.

When $g = G$, the interaction Hamiltonian (2) reduces to:

$$\mathcal{H}_{\text{WLC}}/\hbar = g(\hat{a} + \hat{c}^\dagger)\hat{b}^\dagger + g(\hat{a}^\dagger + \hat{c})\hat{b} + \alpha(\hat{a} + \hat{a}^\dagger)\Phi, \quad (4)$$

and the \mathcal{PT} symmetry emerges. In this case, \mathcal{P} -transformation switches \hat{a} and \hat{c} and \mathcal{T} -transformation switches creation and annihilation operators. Under the joint \mathcal{PT} -transformation, the Hamiltonian keeps its original form. Moreover, in the ideal case when \hat{a}/\hat{c} are lossless, the response of the $\hat{a} + \hat{c}^\dagger$ to the axion driving is inversely proportional to the frequency, thereby achieving a significant enhancement of the signal thereby sensitivity $S_\alpha(\Omega)$ at low frequencies. The conceptual designs and how the system behave under the non-ideal situation where the \hat{a}/\hat{c} possess internal loss and $g \neq G$ has been demonstrated and optimized in [30].

In this paper we generalize this \mathcal{PT} -symmetric design concept to an array of detectors, targeted at further

enhancing the signal-to-noise ratio. Since the coherent length of the axion dark matter signal is typically 10^3 times the Compton length that resonant microwave cavity usually matches, one can upgrade it to a fully- \mathcal{PT} -symmetric setup with multiple probing sensors, which turns out to be more robust.

A chain of \mathcal{PT} -symmetric detector— The advantage of the \mathcal{PT} -symmetric detector design comes from its high response to the signal at low frequencies. Such an advantage can be further enhanced by considering an extension of the model with more \mathcal{PT} -symmetric structures which we named as *chain detector design*, as shown in Fig. (2). The interaction Hamiltonian of this chain detector design is

$$\begin{aligned} \hat{H}_{\text{CD}}/\hbar = & \sum_{i=1}^n g\hat{a}_i\hat{a}_{i+1}^\dagger + G\hat{c}_i\hat{a}_{i+1} \\ & + g\hat{a}_n\hat{b}^\dagger + G\hat{c}_n\hat{b} + \alpha\hat{a}_1\Phi + \text{h.c.} \end{aligned} \quad (5)$$

In case of $g = G$, we have: $g\hat{a}_i\hat{a}_{i+1}^\dagger + G\hat{c}_i\hat{a}_{i+1} \rightarrow g(\hat{a}_i + \hat{c}_i^\dagger)\hat{a}_{i+1}$ and define the \mathcal{PT} -invariant mode $\hat{A}_i \equiv \hat{a}_i + \hat{c}_i^\dagger$. In the lossless case when the external continuous electromagnetic bath \hat{u}_r only couples to the readout \hat{b} mode via strength $\sqrt{2\gamma_r}$, we have the following equations of motion:

$$\begin{aligned} \dot{\hat{A}}_i &= -ig\hat{A}_{i-1}, \quad \dot{\hat{A}}_1 = -i\alpha\Phi, \\ \dot{\hat{b}} &= -\gamma_r\hat{b} - ig\hat{A}_n + \sqrt{2\gamma_r}\hat{u}_r, \quad \hat{v}_r = \hat{u}_r - \sqrt{2\gamma_r}\hat{b}. \end{aligned} \quad (6)$$

In the frequency domain, these equations can be stacked in the following way:

$$\hat{v}_r(\Omega) = \frac{\Omega - i\gamma_r}{\Omega + i\gamma_r}\hat{u}_r(\Omega) - \frac{i\sqrt{2\gamma_r}\alpha\Phi}{\Omega + i\gamma_r} \left(\frac{g}{\Omega}\right)^n. \quad (7)$$

Clearly, there is an enhanced amplification factor $\mathcal{G}^n(\Omega) = (g/\Omega)^n$ due to the chain structure. Thus the low frequency signal response scales as $\sim \Omega^{-n}$ [34], while at the same time, the noise is still at the shot-noise level since $S_{u_r u_r} = 1$ (in principle, this shot noise level can be further reduced via squeezing technology so that $S_{u_r u_r} = e^{-2r_s}$ where r_s is the squeezing degree). The signal power and noise spectrum in this ideal lossless case are given by:

$$\frac{1}{S_\alpha(\Omega)} = \frac{2\gamma_r\alpha^2 S_\Phi(\Omega)}{\gamma_r^2 + \Omega^2} \left(\frac{g^2}{\Omega^2}\right)^n e^{2r_s}. \quad (8)$$

Imperfections and robustness— In practice the lossless condition and the \mathcal{PT} -symmetric condition can not be achieved as ideal, and the robustness of device's sensitivity towards varying of the loss rate and \mathcal{PT} -symmetric condition needs to be taken into account. Let us first consider the case when $g = G$, but there exists

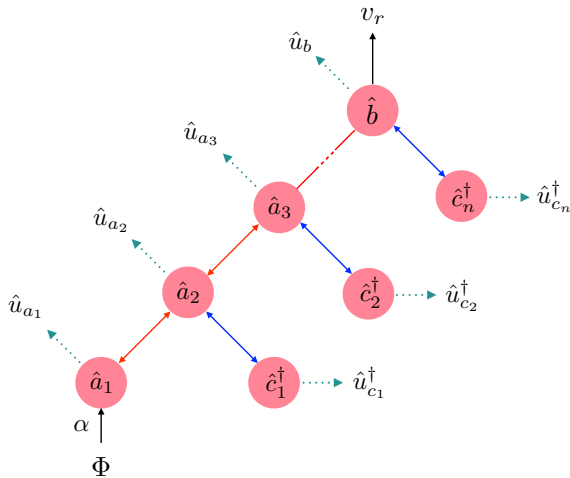


FIG. 2: Chain Detector Configuration, where the red lines represent the beam-splitter type of interaction while the blue lines represent the parametric type of interaction. Each circle represents a degree of freedom of the system and only \hat{a}_1 is driven by the axion signal field. The information of the axion field is detected at the \hat{b} -port.

internal loss $\gamma_{a/c}$ and we assume that the internal loss for each resonator is the same so that $\gamma_a = \gamma_c = \gamma$. The signal enhancement factor in this case would be $\mathcal{G}(\Omega) = g^2/(\gamma^2 + \Omega^2)$ and the signal power $S_{\text{sig}}^{\text{CD}}(\Omega)$, noise spectrum due to the readout $S_r^{\text{CD}}(\Omega)$ and the internal loss $S_{\text{int}}^{\text{CD}}$ now can be written respectively as:

$$S_{\text{sig}}^{\text{CD}}(\Omega) = \frac{2\gamma_r \alpha^2 S_{\Phi}(\Omega)}{(\gamma + \gamma_r)^2 + \Omega^2} \mathcal{G}^n(\Omega), \quad (9)$$

$$S_r^{\text{CD}}(\Omega) = \frac{(\gamma - \gamma_r)^2 + \Omega^2}{(\gamma + \gamma_r)^2 + \Omega^2} S_{u_r}, \quad (10)$$

$$S_{\text{int}}^{\text{CD}}(\Omega) = \frac{4\gamma\gamma_r}{(\gamma + \gamma_r)^2 + \Omega^2} \left[S_{u_b} + \sum_{i=1}^n \mathcal{G}^{n+1-i} (S_{u_{a_i}} + S_{u_{c_i}}) \right], \quad (11)$$

where the noise spectrum $S_{u_{a_i}}, S_{u_{c_i}}$ are the loss contributions from the \hat{a}_i and \hat{c}_i , including both vacuum and thermal fluctuations. Even at $\Omega < \gamma$, as long as $g \gg \gamma$, there is still a significant amplification of the signal power. We can vary the value of γ_r while fixing $g = G$ to optimize the scan-rate in Eq. (1) and the optimized spectrum for $n = 2, 3$ is shown in the Appendix. It turns out that increasing the resonant chain levels could improve the scan-rate R_a by a factor of $(g/\gamma n_{\text{occ}})^{2n/(2n+1)}$, through broadening the range of $S_{\text{int}}^{\text{CD}}(\Omega) \gg S_r^{\text{CD}}(\Omega)$, where n_{occ} is the thermal occupation number.

On the other hand, the mismatch between g and G , which breaks the \mathcal{PT} symmetry, will affect the system response as well and it has been also discussed in [30]. Therefore we also need to test the robustness of the optimized scan-rate and the result is shown in Fig. (3), where

we calculate how the scan-rate ratio $R_{\alpha}(g \neq G)/R_{\alpha}(g = G)$ would change with respect to $\sqrt{g^2 - G^2}$ at zero temperature. In this figure, the scan-rate would drop by half if $g^2 - G^2 \sim 10^5 \gamma^2$ when $g/\gamma = 10^4$, which requires $g - G \ll 5\gamma$. For the system with large g , it could be a fine-tuning problem and thereby the system is less robust towards the $g - G$ mismatch.

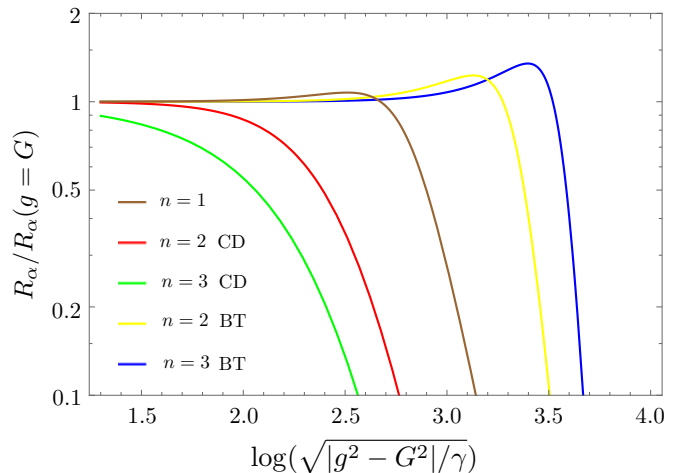


FIG. 3: The effect of \mathcal{PT} symmetry breaking when $g^2 - G^2 > 0$ to the scan-rate of chain detector configuration and binary tree configuration at zero temperature for $g/\gamma = 10^4$.

Binary tree design— An alternative design, with schematic diagram shown in Fig. (4) (in this paper, we call it *binary tree design*), could relieve the problem of robustness shown in the previous section. The corresponding Hamiltonian can be written as:

$$\begin{aligned} \hat{H}_{\text{BT}}/\hbar &= (g\hat{a}_{n1}^\dagger + G\hat{c}_{n1})\hat{b} + \sum_{j=1}^{2^{n-1}} \alpha \hat{a}_{1j} \Phi \\ &+ \sum_{i=2}^n \sum_{j=1}^{2^{n+1-i}} \hat{a}_{ij} (g\hat{a}_{i-1,2j-1}^\dagger + G\hat{c}_{i-1,2j-1}) \\ &+ \sum_{i=2}^n \sum_{j=1}^{2^{n+1-i}} \hat{c}_{ij} (g\hat{a}_{i-1,2j-1}^\dagger + G\hat{c}_{i-1,2j}) + h.c. \end{aligned} \quad (12)$$

It is important to note that in this design, we are allowed to have multiple resonant modes to probe the axions, while in the chain detector, we only have one. Since the typical correlation wavelength of the axion dark matter is much larger than the spatial scale between these resonators, there is a coherent enhancement of signal fields as well as the scan-rate. However, we need a benchmark to compare different device designs [35], and such a benchmark is chosen to be the total signal amplitude at the input. This is to say that when we compare the

chain resonator design and the binary tree design, we set the total signal amplitude to be the same. Practically speaking, it means we can reduce the strength of the background magnetic field in the coupling cavities \hat{a}_{1i} , ($i = 1, \dots, N$) by a factor of N . In this sense, there is no advantage of the binary tree design over the chain detector design when there is no loss and \mathcal{PT} symmetry is strict.

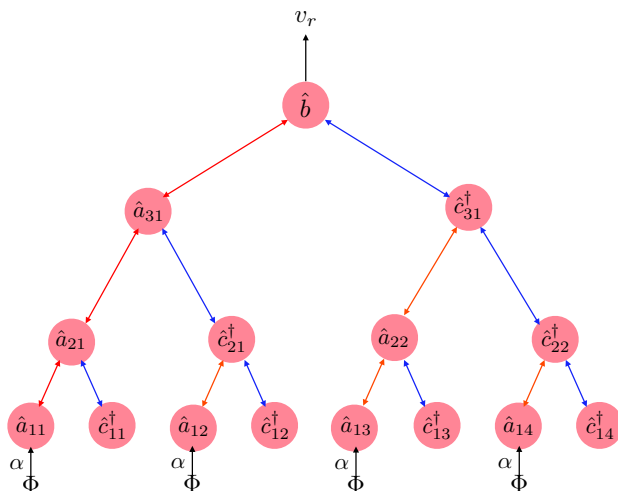


FIG. 4: An example of *binary tree design* with $n = 3$, with red lines denoting beam-splitter-type interaction and blue lines denoting parametric-type interaction. The probing modes to the dark matter are chosen to be the \hat{a}_{1i} modes in the lowest level.

The structure of the interaction between \hat{a}_{ij} and \hat{c}_{ij} renders the Hamiltonian (12) to have a largely enhanced \mathcal{PT} symmetry. It turns out to demonstrate much higher robustness to the $g-G$ mismatch than the resonant chain detector as we can see from Fig. (3), and increasing the level n of the binary tree design also enhances the robustness.

Experimental expectations— We now discuss the application of the \mathcal{PT} -symmetric array to the electromagnetic resonant detectors. These include a microwave cavity embedded in a strong DC magnetic field with the coupling strength $\alpha = g_{\Phi\gamma}\eta B_0\sqrt{m_\Phi V}$, where $g_{\Phi\gamma}$ is the axion-electromagnetic-field coupling, η is the overlapping factor of the cavity mode with the background magnetic field B_0 and V is the cavity volume [6, 7]. We also consider superconducting-LC circuits [8]/superconducting radiofrequency (SRF) cavity [23] embedded in the DC/AC magnetic field with corresponding coupling strength to be $\alpha_{\text{LC}} = g_{\Phi\gamma}B_0V^{5/6}m_\Phi^{3/2}$ and $\alpha_{\text{RF}} = g_{\Phi\gamma}\eta B_0m_\Phi\sqrt{V/\omega_{\text{rf}}}$ respectively, where ω_{rf} is the resonant frequency of the SRF cavity.

The potential physics reach based on the three different types of experiments are shown in Fig. (5) with the integration time distributed for each e-fold in axion mass

to be $t_e = 10^7$ s and signal-to-noise ratio (SNR) reaching 1. In the appendix, we show that SNR is proportional to the square root of the scan-rate in Eq. (1). Thus the enhancement factor for SNR is $(g/\gamma n_{\text{occ}})^{n/(2n+1)}$. Since g cannot be larger than the resonant frequency ω , we take $g = Q_{\text{int}}\gamma$. Thus the high quality factor as well as an almost fixed thermal occupation number of the SRF cavity leads to a much larger enhancement. The benchmark parameters for cavity with DC magnetic field is $V = 1 \text{ m}^3$, $\eta = 1$, $B_0 = 4 \text{ T}$, $T = 10 \text{ mK}$, $Q_{\text{int}} = 10^4$ while the LC circuit only differs by $Q_{\text{int}} = 10^6$ [27]. For SRF, the differences with the traditional cavity is $Q_{\text{int}} = 10^{12}$, $B_0 = 0.2 \text{ T}$, $T = 1.8 \text{ K}$ and the resonant frequency is almost fixed to be $\omega_{\text{rf}} = 2\pi \text{ GHz} + m_\Phi$ [23]. Below kHz, we also include the contribution of the phase fluctuation noise that dominates over the thermal noise, with the overlapping factor between pumping magnetic field and the signal electric field to be $\epsilon_{1d} = 10^{-5}$ and the quality factor of the pumping field to be the same as Q_{int} .

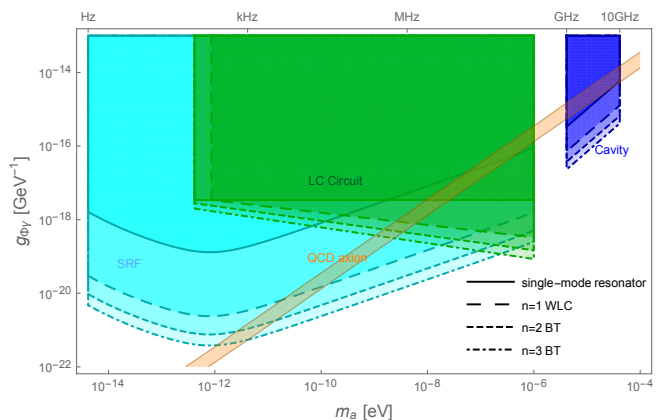


FIG. 5: Physics reach for cavity, LC circuit with DC magnetic field and SRF with AC magnetic field. Here we choose the binary tree detector design as an example (because of its robustness to the $g - G$ mismatch).

Conclusions— In this work, we explore the generalization of the axion detector design assisted with \mathcal{PT} -symmetric quantum amplifier to be a multiple resonant system for the further enhancement of sensitivity. Two generalized scheme configurations are discussed and compared respectively: the *chain detector* configuration and the *binary tree* configuration in terms of the signal and noise response as well as the robustness towards the variation of the optimized system parameters. We found that both of these detector configurations have the potential capability of sensitivity enhancement, while the chain detector configuration is less robust toward the breaking of \mathcal{PT} symmetry compared to the binary tree configuration.

In the end, these improvement of detector capability for constraining the axion mass and the axion-photon

coupling of the design concept in this work for three different types of electromagnetic resonant experiments (cavity, LC circuit with a static magnetic field and SRF with an AC magnetic field) are also discussed. The enhancement to the scan-rate is $\sim (g/\gamma n_{\text{occ}})^{2n/(2n+1)}$. The large quality factor Q_{int} of the SRF thus can lead to a great enhancement and probe most of the QCD axion parameter space above kHz.

Acknowledgements We are grateful to Yanbei Chen, Saptarshi Chaudhuri, Konrad W. Lehnert and Yue Zhao for useful discussions. Y.C. is supported by the China Postdoctoral Science Foundation under Grant No. 2020T130661, No. 2020M680688, the International Postdoctoral Exchange Fellowship Program, and by the National Natural Science Foundation of China (NSFC) under Grants No. 12047557. The research of M.J. is supported by a research grant from Dr. Adrian Langleben, the Veronika A. Rabl Physics Discretionary Fund, and the Estate of Rachel Berson. J.S. is supported by the National Natural Science Foundation of China under Grants No. 12025507, No. 11690022, No.11947302; and is supported by the Strategic Priority Research Program and Key Research Program of Frontier Science of the Chinese Academy of Sciences under Grants No. XDB21010200, No. XDB23010000, and No. ZDBS-LY-7003. Y.C. would like to thank Center for Gravitational Experiment for their kind hospitality.

-
- [1] R. Peccei and H. R. Quinn, *Phys. Rev. Lett.* **38**, 1440 (1977).
- [2] A. Arvanitaki, S. Dimopoulos, S. Dubovsky, N. Kaloper, and J. March-Russell, *Phys. Rev. D* **81**, 123530 (2010), 0905.4720.
- [3] J. Preskill, M. B. Wise, and F. Wilczek, *Phys. Lett. B* **120**, 127 (1983).
- [4] L. Abbott and P. Sikivie, *Phys. Lett. B* **120**, 133 (1983).
- [5] M. Dine and W. Fischler, *Phys. Lett. B* **120**, 137 (1983).
- [6] P. Sikivie, *Phys. Rev. Lett.* **51**, 1415 (1983), [Erratum: *Phys.Rev.Lett.* 52, 695 (1984)].
- [7] P. Sikivie, *Phys. Rev. D* **32**, 2988 (1985), [Erratum: *Phys.Rev.D* 36, 974 (1987)].
- [8] P. Sikivie, N. Sullivan, and D. Tanner, *Phys. Rev. Lett.* **112**, 131301 (2014), 1310.8545.
- [9] S. M. Carroll, G. B. Field, and R. Jackiw, *Phys. Rev. D* **41**, 1231 (1990).
- [10] D. Harari and P. Sikivie, *Phys. Lett. B* **289**, 67 (1992).
- [11] Y. Chen, J. Shu, X. Xue, Q. Yuan, and Y. Zhao, *Phys. Rev. Lett.* **124**, 061102 (2020), 1905.02213.
- [12] P. W. Graham and S. Rajendran, *Phys. Rev. D* **88**, 035023 (2013), 1306.6088.
- [13] D. Budker, P. W. Graham, M. Ledbetter, S. Rajendran, and A. Sushkov, *Phys. Rev. X* **4**, 021030 (2014), 1306.6089.
- [14] M. Jiang, H. Su, A. Garcon, X. Peng, and D. Budker (2021), 2102.01448.
- [15] N. Du et al. (ADMX), *Phys. Rev. Lett.* **120**, 151301 (2018), 1804.05750.
- [16] A. Payez, C. Evoli, T. Fischer, M. Giannotti, A. Mirizzi, and A. Ringwald, *JCAP* **02**, 006 (2015), 1410.3747.
- [17] V. Anastassopoulos et al. (CAST), *Nature Phys.* **13**, 584 (2017), 1705.02290.
- [18] B. T. McAllister, G. Flower, E. N. Ivanov, M. Goryachev, J. Bourhill, and M. E. Tobar, *Phys. Dark Univ.* **18**, 67 (2017), 1706.00209.
- [19] B. M. Brubaker, Ph.D. thesis, Yale U. (2017), 1801.00835.
- [20] S. Lee, S. Ahn, J. Choi, B. R. Ko, and Y. K. Semertzidis, *Phys. Rev. Lett.* **124**, 101802 (2020), 2001.05102.
- [21] S. Chaudhuri, P. W. Graham, K. Irwin, J. Mardon, S. Rajendran, and Y. Zhao, *Phys. Rev. D* **92**, 075012 (2015), 1411.7382.
- [22] J. L. Ouellet et al., *Phys. Rev. Lett.* **122**, 121802 (2019), 1810.12257.
- [23] A. Berlin, R. T. D’Agnolo, S. A. Ellis, C. Nantista, J. Neilson, P. Schuster, S. Tantawi, N. Toro, and K. Zhou, *JHEP* **07**, 088 (2020), 1912.11048.
- [24] M. Malnou, D. Palken, B. Brubaker, L. R. Vale, G. C. Hilton, and K. Lehnert, *Physical Review X* **9** (2019), ISSN 2160-3308.
- [25] L. Krauss, J. Moody, F. Wilczek, and D. E. Morris, *Phys. Rev. Lett.* **55**, 1797 (1985).
- [26] H. Zheng, M. Silveri, R. Brierley, S. Girvin, and K. Lehnert (2016), 1607.02529.
- [27] S. Chaudhuri, K. Irwin, P. W. Graham, and J. Mardon (2018), 1803.01627.
- [28] S. Chaudhuri, K. D. Irwin, P. W. Graham, and J. Mardon (2019), 1904.05806.
- [29] A. Berlin, R. T. D’Agnolo, S. A. Ellis, and K. Zhou (2020), 2007.15656.
- [30] X. Li, M. Goryachev, Y. Ma, M. E. Tobar, C. Zhao, R. X. Adhikari, and Y. Chen (2020), 2012.00836.
- [31] H. Miao, Y. Ma, C. Zhao, and Y. Chen, *Phys. Rev. Lett.* **115**, 211104 (2015), 1506.00117.
- [32] J. Russer and P. Russer (2011), pp. 1–4, ISBN 978-1-4244-5117-3.
- [33] N. Bergeal, R. Vijay, V. E. Manucharyan, I. Siddiqi, R. J. Schoelkopf, S. M. Girvin, and M. H. Devoret, *Nature Physics* **6**, 296 (2010).
- [34] Note that although the signal response gets amplified at low frequencies, the signal decreases faster at high frequency region.
- [35] Another example is in the gravitational wave detectors, to show the advantage of detector upgrades, one usually needs to compare the sensitivity curve of the upgraded detector and the original detector assuming the same intra-cavity power.

Appendix: Optimization of signal-to-noise ratio
 In [23, 27, 28], it was shown that the total signal-to-noise ratio (SNR) for a square-law detection, with an optimized filter chosen, is proportional to

$$\begin{aligned}
 \text{SNR}^2(\gamma_r) &= t_{\text{int}} \int_{-\infty}^{+\infty} d\Omega \left(\frac{S_{\text{sig}}(\Omega, \gamma_r)}{S_{\text{N}}} \right)^2 \\
 &= t_e \frac{\Delta\omega_{sc}}{m_{\Phi}} \Delta\omega_s \left(\frac{S_{\text{sig}}(0, \gamma_r)}{S_{\text{N}}} \right)^2 \\
 &= \frac{t_e \rho_{\text{DM}}^2 Q_{\Phi}}{m_{\Phi}^6} \int_{-\infty}^{+\infty} d\Omega \left(\frac{S_{\text{sig}}(\Omega, \gamma_r)}{S_{\text{N}} S_{\Phi}} \right)^2,
 \end{aligned} \tag{A-1}$$

where $S_{\text{N}} \equiv S_{\text{int}} + S_{\text{r}}$ is the total noise power spectral density (PSD). It is assumed that the scan is performed uniformly in $\log m_{\Phi}$, with the same time t_e distributed for each e -fold in axion mass. $t_{\text{int}} = t_e \Delta\omega_{sc}/m_{\Phi}$ is the integration time within one scan step, required to be larger than the cavity ring-up time-scale and dark matter coherent time $2\pi Q_{\Phi}/m_{\Phi}$. $\Delta\omega_{sc}$ is defined as the single scan step within which the expected SNR of is an $\mathcal{O}(1)$ of the maximum value and $\Delta\omega_s$ is the bandwidth of $(S_{\text{sig}}/S_{\text{N}})^2$. In the case that dark matter bandwidth m_{Φ}/Q_{Φ} is smaller than the sensitivity width of the detector, i.e., the width of $(S_{\text{sig}}/(S_{\text{N}} S_{\Phi}))^2$, one have $\Delta\omega_s = m_{\Phi}/Q_{\Phi}$ and $\Delta\omega_{sc}$ is the sensitivity width. Now it's clear that the quantity needed to be optimized is the integral in the last line of Eq. (A-1), which is the scan-rate in Eq. (1). We parametrize the SNR to be

$$\text{SNR} = \frac{\rho_{\text{DM}} \alpha^2}{m_{\Phi}^3} \sqrt{\frac{Q_{\Phi} t_e}{\gamma}} \widetilde{\text{SNR}}. \tag{A-2}$$

For the chain detector case, using Eq. (9-11), we numerically maximize $\widetilde{\text{SNR}}$ with $n = 1, 2, 3$ at zero temperature and fit optimization conditions for γ_r and the corresponding $\widetilde{\text{SNR}}$:

$$\begin{aligned}
 n = 1 &: \gamma_r = 1.05(g^2\gamma)^{1/3}, \widetilde{\text{SNR}} = 0.70(g/\gamma)^{1/3}; \\
 n = 2 &: \gamma_r = 1.01(g^4\gamma)^{1/5}, \widetilde{\text{SNR}} = 0.70(g/\gamma)^{2/5}; \\
 n = 3 &: \gamma_r = 0.99(g^6\gamma)^{1/7}, \widetilde{\text{SNR}} = 0.70(g/\gamma)^{3/7}.
 \end{aligned} \tag{A-3}$$

The results are shown in the upper panel of Fig. (A-1).

To understand and generalize the optimized $\widetilde{\text{SNR}}$ analytically, one first takes $\gamma_r \simeq (g^{2n}\gamma)^{1/(2n+1)}$ according to the optimization conditions in Eq. (A-3). This makes S_{r} in Eq. (10) to be a flat spectrum, also shown in Fig. (A-2). If the relevant bandwidth in Eq. (A-1) is smaller than g , S_{int} is dominated by the contribution from the lowest level, i.e., $S_{u_{a_1}}$ and $S_{u_{c_1}}$ terms in Eq. (11), and $S_{\text{int}}(\Omega \ll g) \simeq \frac{4\gamma\gamma_r}{(\gamma+\gamma_r)^2+\Omega^2} \left(\frac{g^2}{\gamma^2+\Omega^2} \right)^n$. We can now see that the sensitivity bandwidth $\Delta\omega_{sc}$ in Eq. (A-1) is just

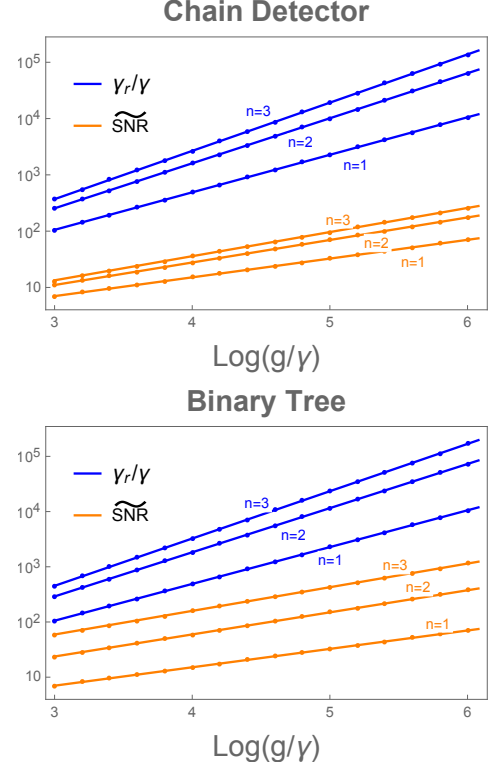


FIG. A-1: Optimization conditions for γ_r when $g = G$ and corresponding $\widetilde{\text{SNR}}$ for chain detector and binary tree haloscope, shown also in Eq. (A-3) and Eq. (A-9).

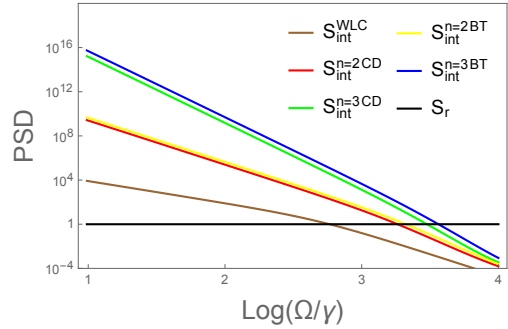


FIG. A-2: The corresponding noise PSD for $n = 1, 2, 3$ at $g/\gamma = 10^4$ under the optimization condition in Fig. (A-1). S_{r} for the three are almost the same.

the range that intrinsic fluctuations S_{int} dominates over the readout noise S_{r} :

$$S_{\text{int}}(\Omega < \Delta\omega_{sc}) > S_{\text{r}}(\Omega < \Delta\omega_{sc}) \simeq 1, \tag{A-4}$$

since $(S_{\text{sig}}/(S_{\text{int}} S_{\Phi}))^2$ remains a constant within the bandwidth. The inequality in Eq. (A-4) leads to

$$\Delta\omega_{sc} \simeq \gamma_r \simeq (g^{2n}\gamma)^{\frac{1}{2n+1}} < g. \tag{A-5}$$

Taking it back to Eq.(A-1), one has:

$$\text{SNR} \simeq \left(\frac{g}{\gamma}\right)^{\frac{n}{2n+1}} \frac{\rho_{\text{DM}}\alpha^2}{m_{\Phi}^3} \sqrt{\frac{Q_{\Phi}t_e}{\gamma}}, \quad (\text{A-6})$$

which matches well with our numerical optimization in Eq. (A-3). For large n , this leads to an enhanced SNR by a factor approaching $(g/\gamma)^{1/2}$.

For the binary tree case, taking $g = G$ and all the intrinsic dissipation coefficients to be universal, one can calculate the signal and the noise PSD:

$$\begin{aligned} S_{\text{sig}}^{\text{BT}}(\Omega) &= \frac{\gamma_r \alpha^2 S_{\Phi}(\Omega)}{2((\gamma + \gamma_r)^2 + \Omega^2)} \left(\frac{4g^2}{\gamma^2 + \Omega^2}\right)^n; \quad (\text{A-7}) \\ S_{\text{int}}^{\text{BT}}(\Omega) &= \frac{4\gamma\gamma_r}{(\gamma + \gamma_r)^2 + \Omega^2} \left(S_{u_b} \right. \\ &+ \sum_{i=1}^n \sum_{j=1}^{2^{n+1-i}} \left(\frac{g^2}{\gamma^2 + \Omega^2}\right)^{n+1-i} S_{u_{a_{ij}}} \\ &+ \left. \sum_{i=1}^n \sum_{j=1}^{2^{n+1-i}} \left(\frac{g^2}{\gamma^2 + \Omega^2}\right)^{n+1-i} S_{u_{c_{ij}}} \right) (\text{A-8}) \end{aligned}$$

while the readout noise PSD remains the same as Eq. (10). There is an enhancement of 2^{2n-2} compared to the chain detector in Eq. (9) with single sensor. On the other hand, each mode of the intrinsic noise is incoherent and the PSD at each layer i is counted by a factor of the number of the same type of the modes in that layer, 2^{n+1-i} , compared to Eq. (11).

Similarly, one optimizes and fits the $\widetilde{\text{SNR}}$ numerically at zero temperature

$$\begin{aligned} n = 2 : \quad \gamma_r &= 1.15(g^4\gamma)^{1/5}, \quad \widetilde{\text{SNR}} = 1.49(g/\gamma)^{2/5}; \\ n = 3 : \quad \gamma_r &= 1.21(g^6\gamma)^{1/7}, \quad \widetilde{\text{SNR}} = 3.07(g/\gamma)^{3/7}, \end{aligned} \quad (\text{A-9})$$

which are shown in the lower panel of Fig. (A-1). As expected, there is an 2^{n-1} enhancement due to the multi probing sensors:

$$\text{SNR} \simeq 2^{n-1} \left(\frac{g}{\gamma}\right)^{\frac{n}{2n+1}} \frac{\rho_{\text{DM}}\alpha^2}{m_{\Phi}^3} \sqrt{\frac{Q_{\Phi}t_e}{\gamma}}. \quad (\text{A-10})$$

We also optimize $\widetilde{\text{SNR}}$ with both γ_r and $g^2 - G^2$ taken as free parameters, shown in Fig. (A-3) and the corresponding noise PSD is in Fig. (A-4). In the binary tree case, the optimized condition is $g^2 - G^2 \simeq \gamma_r^2 \simeq (g^{2n}\gamma)^{1/(2n+1)}$. Thus a small deviation from the optimized value of $g^2 - G^2$ can lead to negligible impact on the SNR and is indeed more robust than the chain detector when $g^2 - G^2$ needs to be highly fine-tuned.

In the presence of large thermal occupation number $n_{\text{occ}} \equiv 1/2 + 1/(e^{\omega/T} - 1)$, the thermal noise is dominant for each intrinsic noise PSD $S_u = n_{\text{occ}} \simeq T/\omega$.

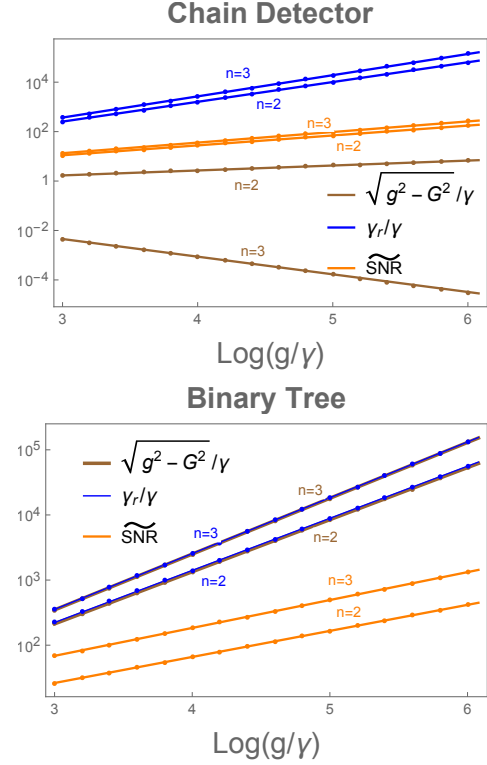


FIG. A-3: Optimization conditions and $\widetilde{\text{SNR}}$ with both γ_r and $g^2 - G^2$ being free parameters for both chain detector and binary tree haloscope.

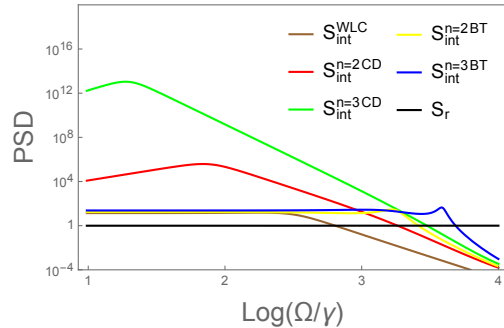


FIG. A-4: The corresponding noise PSD for $n = 1, 2, 3$ at $g/\gamma = 10^4$ under the optimization condition in Fig. (A-3). The PSD of binary tree are flatter compared to the one of chain detector.

For SNR, the finite temperature effect is equivalent to replacing $g^{2n} \rightarrow g^{2n} n_{\text{occ}}$, with new optimized condition $\gamma_r \simeq (g^{2n} \gamma n_{\text{occ}})^{1/(2n+1)}$, and dividing the whole SNR by n_{occ} . For binary tree, Eq. (A-10) becomes

$$\text{SNR}(T \gg \omega) \simeq 2^{n-1} \left(\frac{g}{\gamma n_{\text{occ}}}\right)^{\frac{n}{2n+1}} \frac{\rho_{\text{DM}}\alpha^2}{m_{\Phi}^3} \sqrt{\frac{Q_{\Phi}t_e}{\gamma n_{\text{occ}}}}. \quad (\text{A-11})$$

In the case of microwave cavity with DC magnetic field,

the thermal noise is negligible with $T = 10$ mK and respectively.

$$\text{SNR}_{\text{cavity}} = 2^{n-1} \left(\frac{g}{\gamma} \right)^{\frac{n}{2n+1}} \frac{\rho_{\text{DM}} g_{\Phi}^2 \eta^2 B_0^2 V}{m_{\Phi}^2} \sqrt{\frac{Q_{\Phi} Q_{\text{int}} t_e}{m_{\Phi}}}. \quad (\text{A-12})$$

For the LC circuit and SRF case, the SNR in the thermal noise limit are given by

$$\text{SNR}_{\text{LC}} = 2^{n-1} \left(\frac{gm_{\Phi}}{\gamma T} \right)^{\frac{n}{2n+1}} V^{\frac{5}{3}} g_{\Phi}^2 B_0^2 \rho_{\text{DM}} \sqrt{\frac{Q_{\Phi} Q_{\text{int}} t_e}{T}}, \quad (\text{A-13})$$

$$\text{SNR}_{\text{SRF}} = 2^{n-1} \left(\frac{g\omega_{\text{rf}}}{\gamma T} \right)^{\frac{n}{2n+1}} \frac{\rho_{\text{DM}} g_{\Phi}^2 \eta^2 B_0^2 V}{m_{\Phi} \omega_{\text{rf}}} \sqrt{\frac{Q_a Q_{\text{int}} t_e}{T}}. \quad (\text{A-14})$$